NANO LETTERS

Letter

pubs.acs.org/NanoLett

Twin-Free GaAs Nanosheets by Selective Area Growth: Implications for Defect-Free Nanostructures

Chun-Yung Chi,*[,†,∥] Chia-Chi Chang,[‡,∥] Shu Hu,[⊥,#] Ting-Wei Yeh,[§,∥] Stephen B. Cronin,[†,‡,∥] and P. Daniel Dapkus[†,‡,∥]

[†]Ming Hsieh Department of Electrical Engineering, [‡]Department of Physics & Astronomy, [§]Mork Family Department of Chemical Engineering and Material Science, and [∥]Center for Energy Nanoscience, University of Southern California, Los Angeles, California, 90089, United States

[⊥]Division of Chemistry and Chemical Engineering and [#]Joint Center for Artificial Photosynthesis (JCAP), California Institute of Technology, Pasadena, California, United States

Supporting Information

ABSTRACT: Highly perfect, twin-free GaAs nanosheets grown on (111)B surfaces by selective area growth (SAG) are demonstrated. In contrast to GaAs nanowires grown by (SAG) in which rotational twins and stacking faults are almost universally observed, twin formation is either suppressed or eliminated within properly oriented nanosheets are grown under a range of growth conditions. A morphology transition in the nanosheets due to twinning results in surface energy reduction, which may also explain the high twin-defect density that occurs within some III−V semiconductor nanostructures, such as GaAs nanowires. Calculations suggest that the surface energy is significantly reduced by the formation of {111}-plane bounded tetrahedra after the morphology transition of nanowire structures. By contrast, owing to the formation of two vertical {1$\bar{1}$0} planes which comprise the majority of the total surface energy of nanosheet structures, the energy reduction effect due to the morphology transition is not as dramatic as that for nanowire structures. Furthermore, the surface energy reduction effect is mitigated in longer nanosheets which, in turn, suppresses twinning.

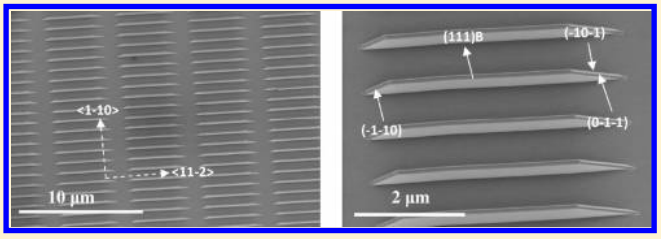

KEYWORDS: *GaAs, nanosheet, defect-free, twin-free, selective-area-growth, MOCVD*

III−V materials have been used in many applications such as logic gates,[1] solar cells,[2,3] and photodetectors[4] because of their superior electrical and optical properties. III−V semiconductor nanowires have been proposed and gained a great deal of attention in recent years owing to their potential to provide improved optical or electrical properties over their bulk counterparts. As a result of their small contact area with the substrate, nanowires can relax the strain due to heteroepitaxy and avoid the formation of dislocations between lattice-mismatched materials. Two growth techniques are widely used to grow III−V nanowires: vapor−liquid−solid (VLS) and selective area growth (SAG). Metal droplets, materials with low eutectic point such as Au, are required in VLS growth to serve as a catalyst to incorporate the precursors from the vapor phase into the liquid phase at low temperatures. The dissolved group-III and group-V atoms in the metal droplets then precipitate at the metal/substrate boundary and deposit a thin layer of material underneath the metal droplets. SAG, on the other hand, is carried out on a nanopatterned substrate at higher temperatures that allow vapor phase precursors to pyrolyze either homogeneously or heterogeneously at the substrate surface via a vapor−solid transition resulting in layer growth without the need of a metal catalyst.

Nanowires (NWs) grown by either technique are characterized by transmission electron microscopy (TEM) to show no dislocations even for highly mismatched NW/substrate pairs.[5,6] However, defects such as stacking-faults and twin defects are commonly observed[7,8] in these structures for most growth conditions and processes. Some studies[9−12] have shown that the existence of twins will reduce carrier lifetime and diffusion length which may deteriorate the optoelectronic properties of twinned nanowires. To minimize these deleterious effects, variations in the growth kinetics of III−V nanowires have been studied to eliminate twins within nanowires. For example, two temperature growth,[13,14] rapid growth,[15] and V/III ratio controlling methods[16] have been demonstrated VLS growth using MOCVD (metal−organic chemical vapor deposition) to reduce twin density within nanowires, and the resulting twin-free nanowires did exhibit better electric properties than twinned nanowires.[9,17] Stacking-fault-free III−V nanowires grown by gold-catalyzed VLS growth using MBE have also been reported.[18,19] Unfortunately there are no

Received: February 12, 2013
Revised: April 17, 2013
Published: May 1, 2013

dx.doi.org/10.1021/nl400561j | *Nano Lett.* 2013, 13, 2506−2515

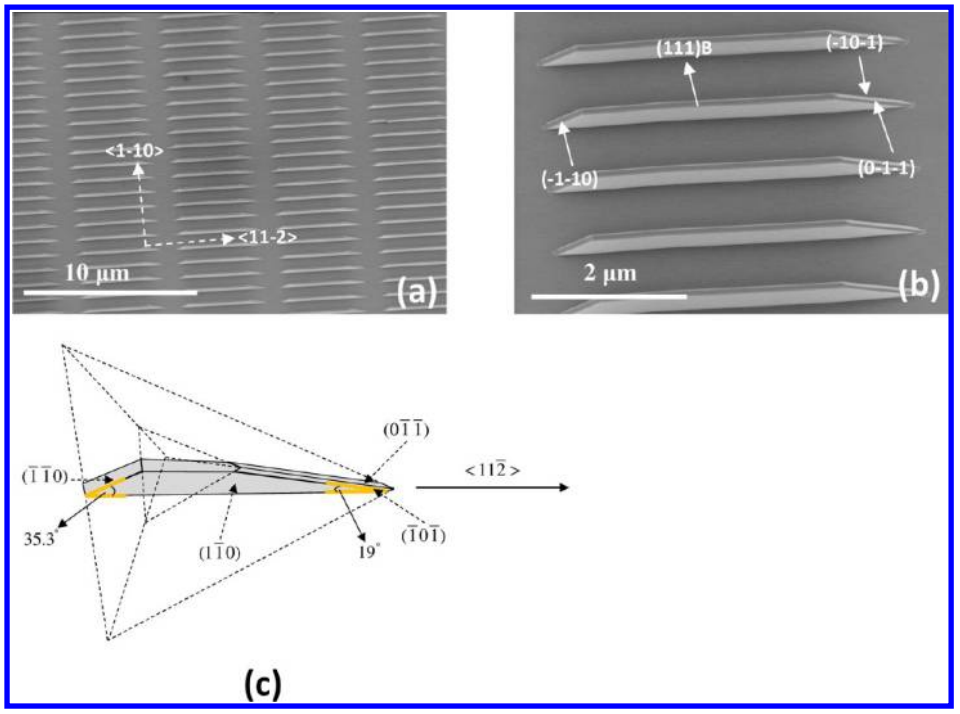

Figure 1. (a) Macroscopic SEM image of nanosheet arrays. Nanostripe pattern is 5 μm long and parallel to $\langle 11-2 \rangle$ direction. (b) Microscopic SEM image of a single nanosheet. The inclined surfaces of the nanosheets are three {110} planes. (c) Schematic diagram of a nanosheet as part of a $\langle 11-2 \rangle$-oriented tetrahedron.

demonstrations of stacking-defect-free nanowires grown by SAG techniques to our knowledge. This is of particular importance for GaAs and alloys based on it, because they are attractive materials for stacked, multiple bandgap solar cells where the ability to form abrupt interfaces and both group III and group V alloys by SAG are enabling characterisitcs.

Ikejiri et al.[20] proposed a model for the SAG growth of nanowires which suggested that twin formation was an inherent part of the nanowire formation. In this model, nucleation on the (111)B plane predominantly occurs by the formation of tetrahedra with {110} surfaces whose long axes are aligned along either the $\langle 11\bar{2} \rangle$ or the $<\bar{1}\bar{1}2>$ direction during the initial stage of nanowire growth. A rotational twin is developed whenever the nucleus on the (111)B surface switches between these two tetrahedral nucleation growths. In a subsequent article by Yoshida et al.,[21] the kinetics of twin formation were studied for different growth conditions and diameters of mask openings to assess the effects of these parameters on the formation of twins. In their study, no variation of the SAG growth conditions or diameter of openings resulted in elimination of twins within SAG nanowires. Although the study provided preliminary information about twin development within nanowires, several phenomena have not been fully explained and understood: for example, why the $\{\bar{1}\bar{1}0\}$ planes of the tetrahedral nuclei vanish when they reach the boundary of the pattern, and how $\{1\bar{1}0\}$ vertical side walls that seem to define the nanowire sidewalls are formed. Similarly, why is the twin density so high in SAG nanowires, and is there a way to form twin-free nanowires? Finally, direct proof of the correlation between the formation of twins and rotation of tetrahedra was not shown.

In this paper, we investigate the influence of the substrate pattern and subsequent nanostructure shapes on the formation of twins in the SAG nanostructures of III−V compound semiconductors. In the process we have discovered a defect-free nanostructure—the nanosheet—which may have its own applications in electronic and optoelectronic technologies. In particular, we employ nanoscale stripe patterns rather than round patterns to form GaAs nanosheets in which twinning is greatly inhibited. The twin-free GaAs nanostructure demonstrated herein is, to our knowledge, unique and the characteristics of its growth morphology solidifies the model of twin development in SAG nanostructures. Since SAG III−V nanowires all exhibit high twin density, the idea of using nanosheet structure to eliminate twins either thermodynamically or kinetically may help to achieve other twin-free III−V nanostructures grown by this technique.

Growth Method. Selective area growth was employed to fabricate nanosheets on GaAs (111)B substrates. Previous studies[22] of III−V SAG nanowires have shown that vertical GaAs nanowires can only be grown along this orientation owing to the surface reconstruction properties of III−V materials. The substrate preparation for nanosheet growth is the same as for nanowires: First, a thin layer of SiN_x was deposited onto the (111)B GaAs substrate by plasma enhanced chemical vapor deposition (PECVD). The thickness of SiN_x mask was around 28 nm. Nanoscale stripes were patterned onto the substrate by electron-beam lithography, and reactive ion etching was used to transfer patterns from the photoresist into the SiN_x mask. The orientation of 5 μm long, 100 nm wide stripes was patterned parallel to the $\langle 11\bar{2} \rangle$ direction. The nanosheet growth was carried out on these samples using a vertical, showerhead, low-pressure metal−organic chemical vapor deposition (MOCVD) reactor. The growth pressure was 0.1 atm, and the precursors for group III and group V materials were trimethylgallium (TMGa) and arsine (AsH_3), respectively. The nanosheets were grown in a hydrogen ambient using a V/III ratio of 6 or less for 30 min at 790 °C. The partial pressure of TMGa and AsH_3 were 3.745×10^{-7} atm and 2.392×10^{-6} atm, respectively, unless otherwise noted.

dx.doi.org/10.1021/nl400561j | Nano Lett. 2013, 13, 2506−2515

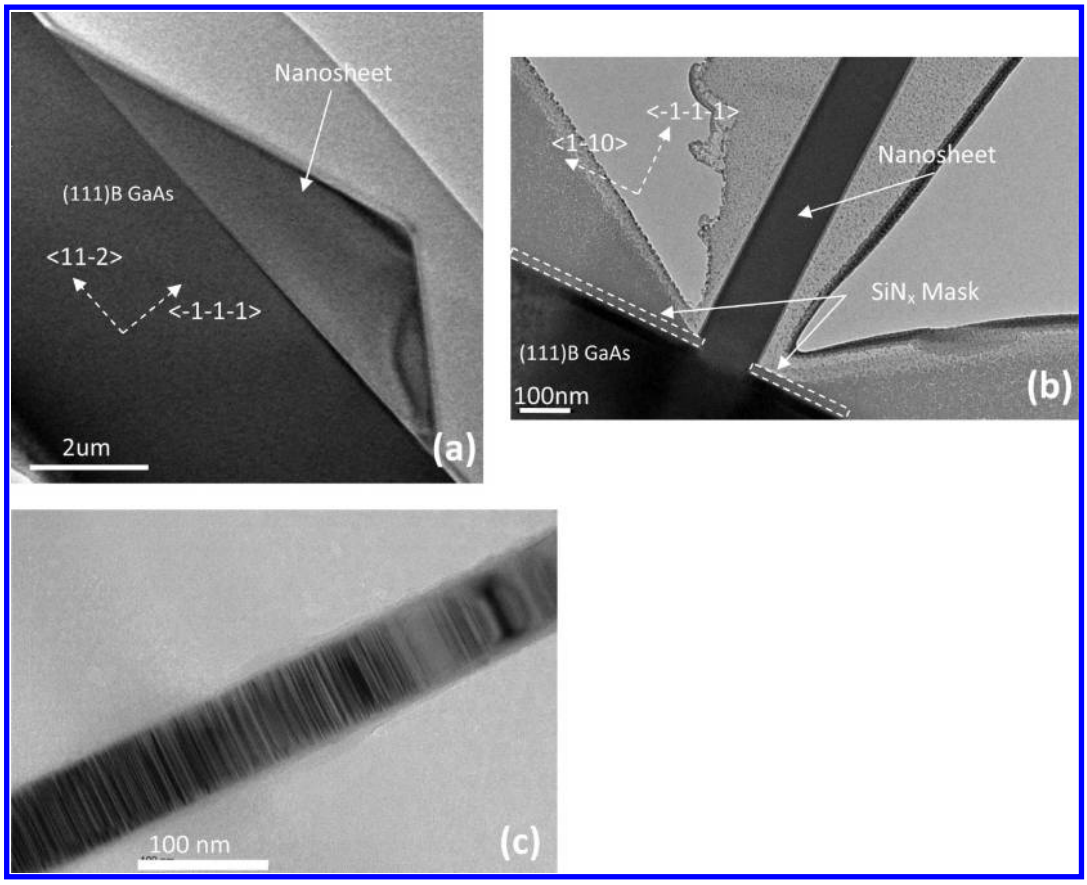

Figure 2. (a) Cross-section TEM image of a nanosheet from ⟨1−10⟩ zone axis. (b) Cross-section TEM image of a nanosheet from ⟨11−2⟩ zone axis. (c) Cross-section TEM of a nanowire at ⟨1−10⟩ zone axis.

Experimental Results. Figure 1a,b shows the scanning electron microscope (SEM) images of nanosheet array samples grown with nanostripes oriented along $\langle 11\bar{2}\rangle$ directions. The length of nanosheets is about 5 μm, and the thickness is around 120 nm. The predominant facets exposed on the nanosheet elements are five equivalent {110} planes: two vertical $(1\bar{1}0)$ planes, and three inclined $(\bar{1}\bar{1}0)$ planes; and the (111)B plane as top surface as shown in Figure 1b. The $\langle 11\bar{2}\rangle$ oriented nanostripes shown here were chosen to coincide with the orientations of the tetrahedral nuclei observed in the studies conducted by Ikejiri et al.[20] and Yoshida et al.[21] In those studies, early stage nuclei grown in small openings were tetrahedra bounded by three {110} planes aligned preferentially with the long axis of the tetrahedra along either the $\langle 11\bar{2}\rangle$ or the $\langle \bar{1}\bar{1}2\rangle$ direction. In the case of nanostripe patterns, the resultant growths oriented along the $\langle 11\bar{2}\rangle$ direction retain the (111)B top surface while the sides are defined by {110} planes as shown in Figure 1c. The nanosheets can be seen as part of a $\langle 11\bar{2}\rangle$ tetrahedron structure with two inclined angles of 19°and 35.3°.

Cross-sectional transmission electron microscopy (TEM) was performed to investigate the crystal structure of the as-grown nanosheets. Cross-sectional TEM images of nanosheets at the $(1\bar{1}0)$ and the $(11\bar{2})$ zone axes are shown in Figure 2a,b, respectively. Figure 2c shows the TEM image of a typical nanowire grown by SAG using similar procedures but employing circular patterns instead of nanostripe patterns. The growth conditions for forming the nanowires are described in a previous publication.[23] A high density of twins is observed within the nanowire structure, while no twins exist within the nanosheets. From the TEM results in Figure 2, the shape and orientation of the patterns seem to play an important role in twin formation within nanostructures thus providing a growth window for twin-free SAG nanosheets.

To investigate the growth window for twin-free GaAs nanosheets, nanosheets were grown under different V/III as shown in Figure 3a−c. In Figure 3a−c, the TMGa flow rate is fixed and only arsine flow rate is changed; the V/III ratios for these three samples are 434, 26, and 6 for Figure 3a, b, and c, respectively. The lateral growth of nanosheets is reduced as the arsine flow rate decreases. Also with higher arsine flow rate, the uniformity of nanosheets becomes worse, and facets other than {110} surfaces are formed as shown in the white circle region in Figure 3a. Because twin-free nanosheets are enclosed by five {110} planes as shown in Figure 1b, it is possible that surfaces other than {110} planes arise from the merging of $\langle 11\bar{2}\rangle$ and $\langle \bar{1}\bar{1}2\rangle$ oriented tetrahedral nuclei. When the arsine flow rate is reduced, only five equivalent $\{\bar{1}\bar{1}0\}$ surfaces are formed. Perfect, uniform nanosheets are formed when V/III ratio is reduced to 6. If the growth time is increased while V/III ratio is fixed at 6, the inclined surfaces of nanosheets are terminated at the tips and thus forming sail-like nanosheets, as shown in Figure 3e. However, some nanosheets show a rotated triangular shape near their tips as shown in the circled regions. The rotated triangular tips can be eliminated with increased TMGa flow rates as shown in Figure 3d. Since nanosheets can be treated as a segment of $\langle 11\bar{2}\rangle$ tetrahedra, the rotation of its triangular shape suggests the development of a twin at the tip of the nanosheets, as proposed for nanowires in Ikejiri's[20] model.

dx.doi.org/10.1021/nl400561j | Nano Lett. 2013, 13, 2506−2515

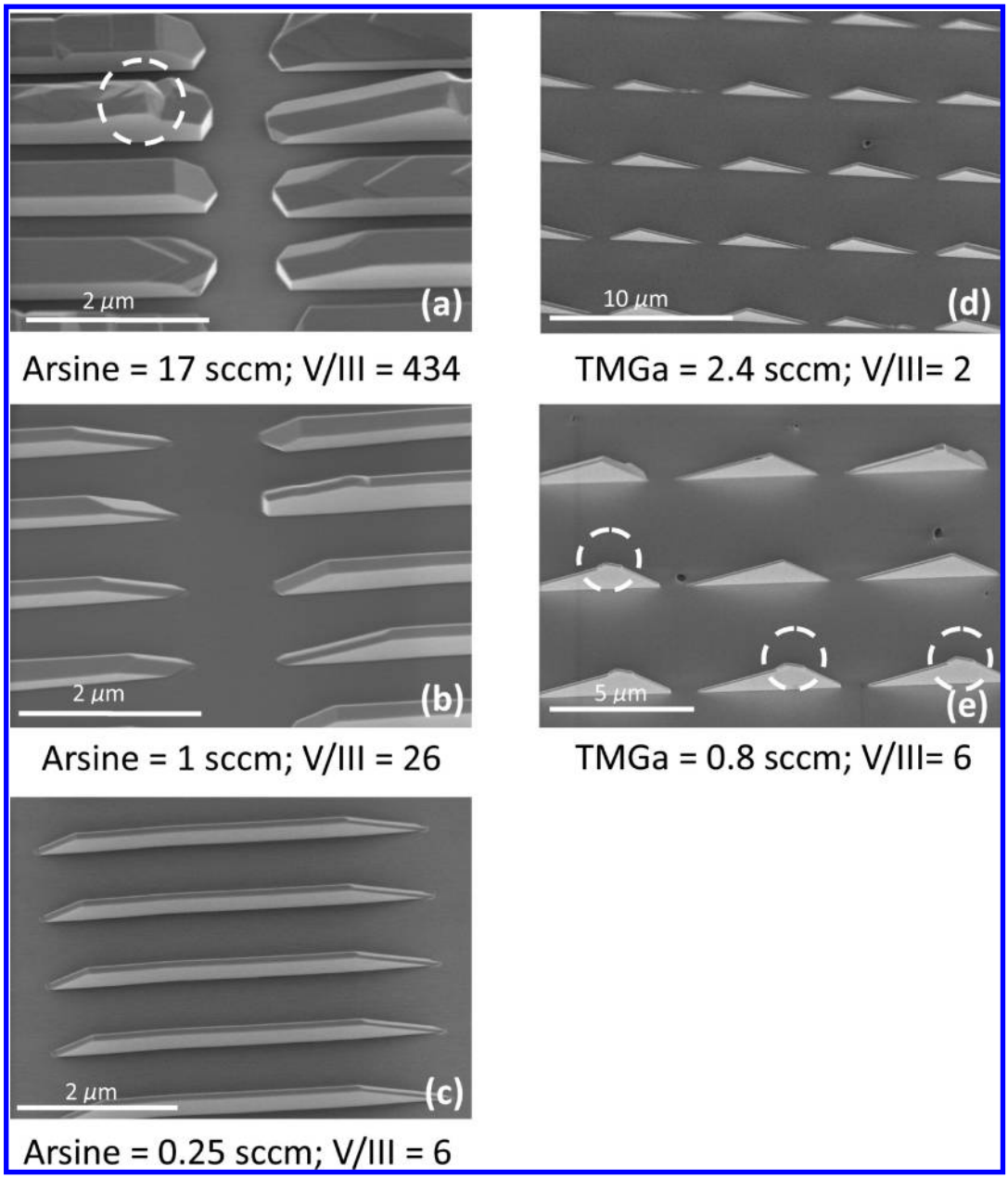

Figure 3. (a–c) SEM images of nanosheets grown under different growth conditions. (d) Nanosheets growth with increased TMGa flow rate which shows suppression of rotated triangular tip. (e) Nanosheets growth under V/III = 6 shows rotated triangular near their tips.

Figure 4a shows the cross-sectional TEM image of the rotated-tip nanosheet in Figure 3e along the $\langle 1\bar{1}0\rangle$ zone axis. According to the TEM image, the nanosheet can be interpreted as stacking of two triangles with a boundary line between them. Figure 4b shows a high-resolution TEM (HRTEM) image near the boundary line in the square region in Figure 4a. As shown in Figure 4b, the atomic arrangements in the two sections are the mirror images of one another, which is also confirmed by the fast Fourier transform (FFT) images of the different regions shown in Figure 4c–e. Figure 4d shows the FFT images of atomic arrangements near the boundary line, an overlap of Figure 4c and e; the extra diffraction spots at the 1/3 of the original reflections in Figure 4c arise from twinning within the nanosheet. The boundary line in Figure 4a is a rotational twin plane near the tip of the nanosheet. Moreover, by measuring the angles of the inclined facets on the two stacking triangles in Figure 4a, the upper triangle is rotated by 180° relative to the bottom triangle. Therefore, the upper triangle can be assigned as part of a $\langle \bar{1}\bar{1}2\rangle$ tetrahedral structure, and the bottom triangle is part of a $\langle 11\bar{2}\rangle$ tetrahedral structure. Combining the TEM and SEM characterizations, once a twin is developed, the surface morphology of nanosheets are altered by the twin formation resulting in a 180° rotation of the triangles near the tip. Such behavior agrees with Ikejiri's[20] model for a nanowire in which twins are developed between the $\langle 11\bar{2}\rangle$ and $\langle \bar{1}\bar{1}2\rangle$ nuclei that subsequently form on the (111)B plane.

Another change which comes after twin formation is the facet transition of the bottom triangle growth: in Figure 4a, before twin was developed, the initial triangle growth with two inclined angles of ~19°and ~33.58° enclosed by white dotted lines was grown; one of its inclined angles increased from ~33.58° to ~68.07° corresponding to a transition of the inclined surface from a $(\bar{1}\bar{1}0)$ plane to a (111)A plane after twin formation. The growth mechanism of the twinned nanosheet

dx.doi.org/10.1021/nl400561j | *Nano Lett.* 2013, 13, 2506–2515

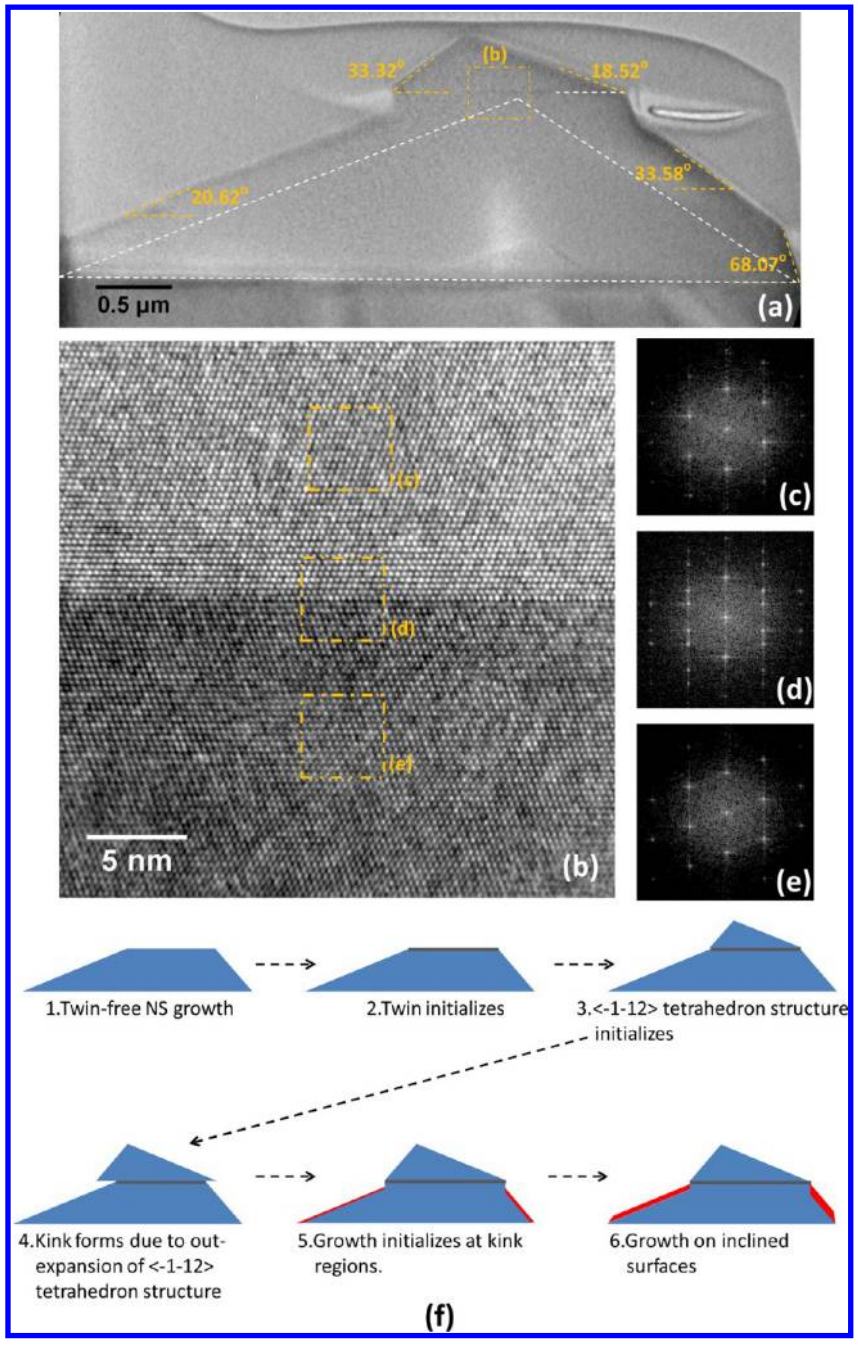

Figure 4. (a) TEM image of cross-section nanosheet along ⟨1−10⟩ direction. The nanosheet is composed of two stacking triangles; the upper triangle is 180° rotated with similar feature of the beneath one. (b) HRTEM image of the boundary between beneath and upper triangles. Stacking sequences of GaAs are different at the two sides of the boundary which implies that this boundary is actually a twin plane. (c−e) FFT images of different regions near the twin plane. (f) Growth mechanism of twinned nanosheets.

can be deduced from the transition morphology of the nanosheets as shown in Figure 4f. First, a twin-free nanosheet which is part of a $\langle 11\bar{2}\rangle$ tetrahedron structure forms. As the inclined facets approach the pinch-off point, a single twin is initialized on the top of (111)B surface as the second step in the process. After a single twin is initialized, the nucleation change from a $\langle 11\bar{2}\rangle$ tetrahedron to a $\langle \bar{1}\bar{1}2\rangle$ tetrahedron, and a 180° rotated triangle growth is formed which is the third step. After that, kinks are formed on the two inclined surfaces of nanosheet which arise from the outward expansion of the upper triangle growth on the plateau as shown in the schematic of the fourth step. In the fifth step, growth starts to initialize in the kink regions. In twin-free nanosheets, the growth rates on the two inclined surfaces are very slow; however, once kinks are formed, they can serve as additional sites to promote epitaxial regrowth on the inclined surfaces of the nanosheets. In the sixth step, due to the confinement of the pattern, the growth on the inclined surfaces will not extend to the masked region. Thus, (111)A surfaces (with lower surface energies than (110) surfaces) are the preferred terminating surfaces under SAG conditions once a twin is formed.

Nanosheet growths on specifically designed nanostripe patterns were also studied. Figure 5a shows nanosheets growth on different lengths of nanostripe patterns. Sail-like nanosheets

dx.doi.org/10.1021/nl400561j | Nano Lett. 2013, 13, 2506−2515

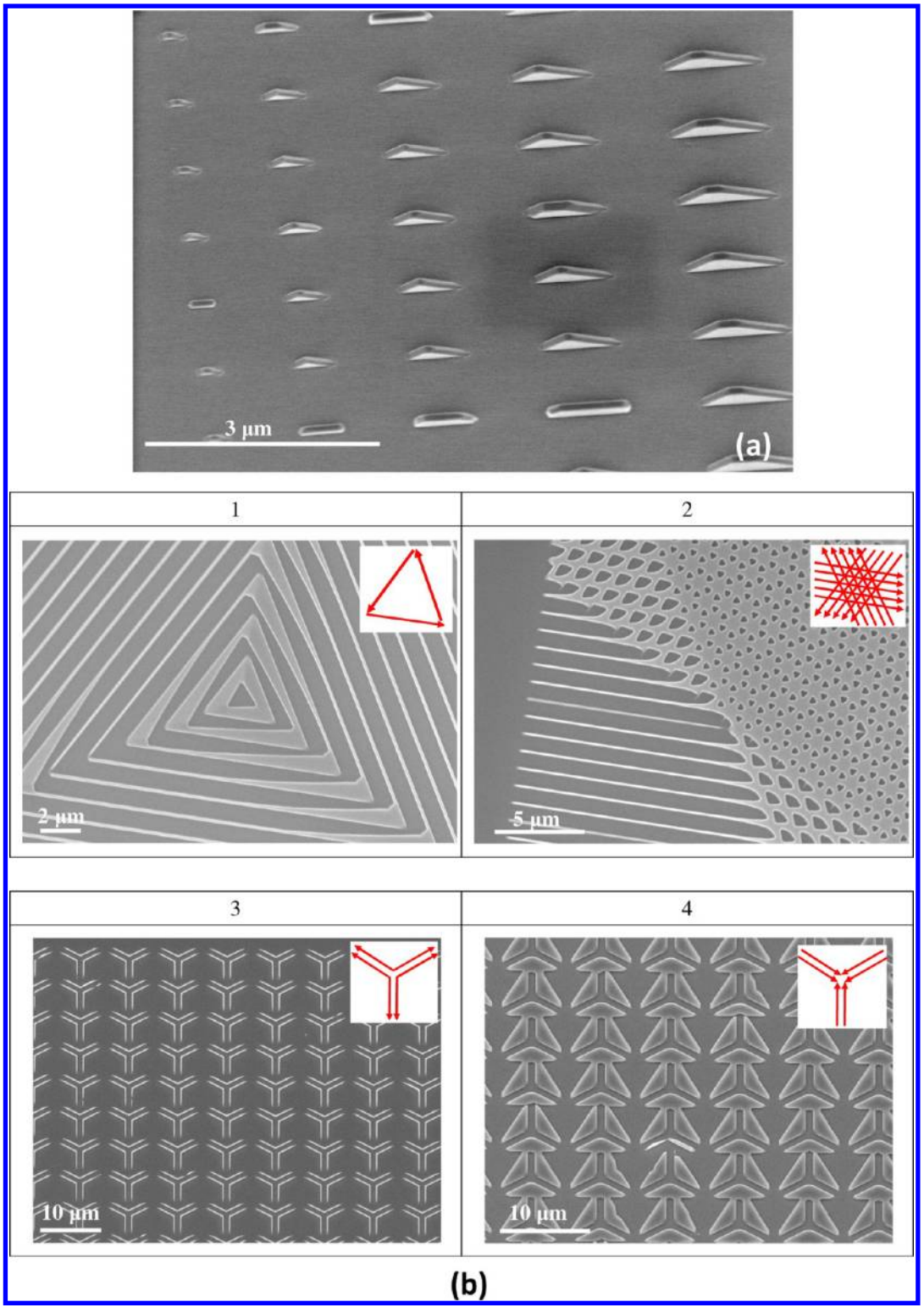

Figure 5. (a) Nanosheets growth on different length of nanostripe patterns. (b) SEM images of nanosheets growth on different nanostripe patterns. Schematics of nanostripe patterns for nanosheets are shown in the insets.

are formed within shorter nanostripe pattern, while longer nanostripe patterns still keep a (111)B plateau on the top surface. The inclined {110} surfaces of nanosheets self-limit the height of nanosheets once the two sides of inclined surfaces are pinched off at the tip. Given enough growth time, the height of nanosheet is eventually determined by the length of the nanostripe pattern; this means the longer the nanostripe pattern is, the taller the nanosheets are as seen in Figure 5a.

Specifically oriented nanostripe patterns shown in Figure 5b were attempted to eliminate the inclined $\{\bar{1}10\}$ surfaces, and their corresponding growth results are shown in Figure 5b. In these subimages, the direction of the arrow denotes three equivalent $\langle 11\bar{2}\rangle$ directions on 3-fold symmetric (111)B GaAs

dx.doi.org/10.1021/nl400561j | *Nano Lett.* 2013, 13, 2506−2515

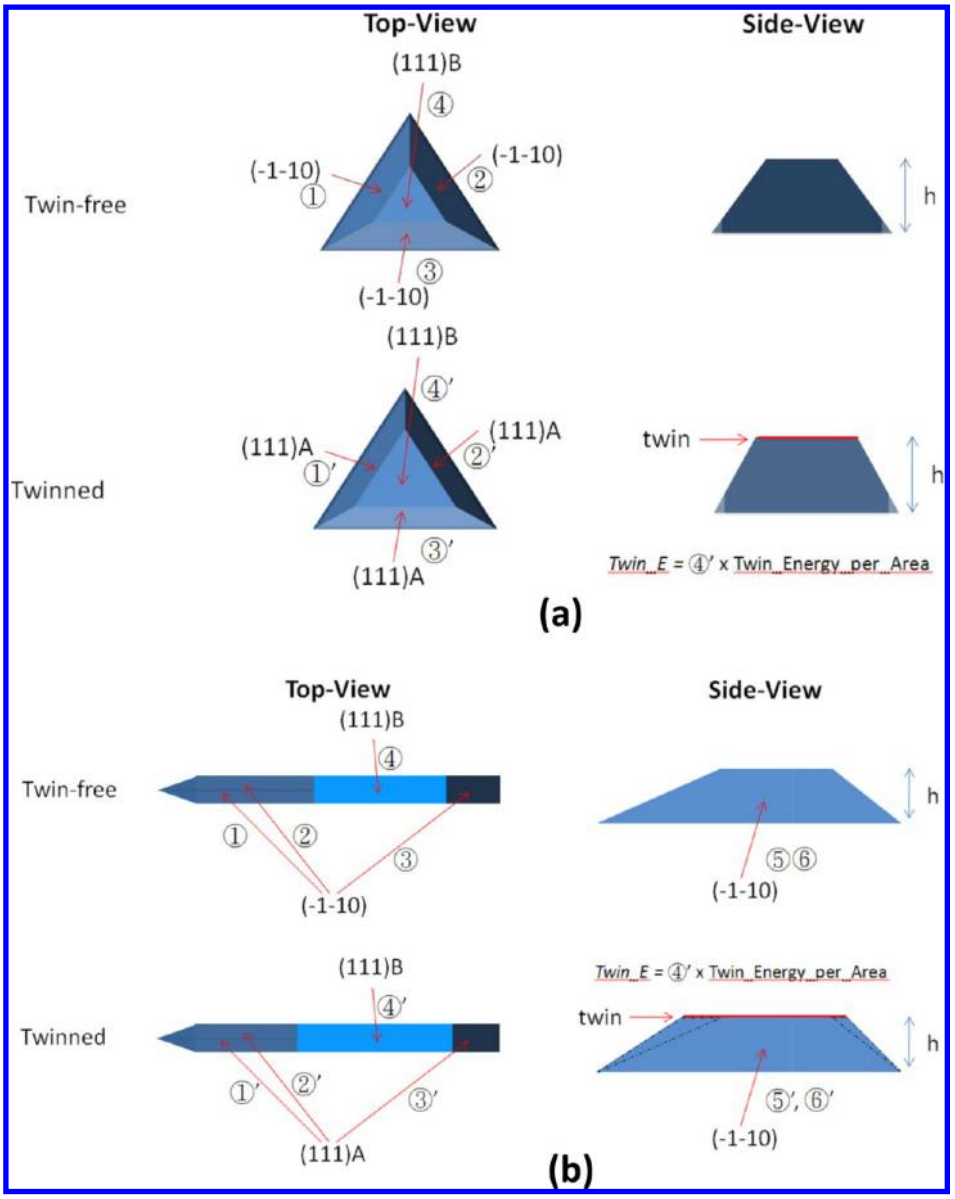

Figure 6. (a) Schematic diagrams of twin-free and twinned cases for a nanowire structure. (b) Schematic diagrams of twin-free and twinned cases for a nanosheet structure.

substrate. In the first pattern, the $\langle 11\bar{2}\rangle$ side and $\langle \bar{1}\bar{1}2\rangle$ side of different nanosheets intersect. As can be seen, the lateral growth is enhanced at these intersections. Similar behavior also occurs in the second pattern: vertical side-walls of nanosheets disappear due to serious lateral growth and nanosheets coalesce with one another other over the mask region. The intersection of different sides of nanosheets exhibited distinctive growth behavior: as shown in the third and fourth pattern, when two $\langle \bar{1}\bar{1}2\rangle$ sides of neighboring nanosheets intersect, lateral growth is still limited by the nanostripe pattern; on the other hand, if two $\langle 11\bar{2}\rangle$ sides of neighboring nanosheets intersect, significant lateral growth is observed. Significant lateral growth was observed as long as the $\langle 11\bar{2}\rangle$ side of nanosheet intersects with any side of another nanosheet as shown in the first and fourth pattern. Due to the differences in lateral growth rate at the intersection of nanosheets, nanostripe patterns could be used to achieve various nanostructures; for example: a thin, twin-free GaAs layer could possibly be grown by intersecting the $\langle 11\bar{2}\rangle$ sides of nanosheets as shown in the second pattern. In addition, taller nanosheets could be formed by intersecting two $\langle \bar{1}\bar{1}2\rangle$ sides of different nanosheets as shown in the third pattern. By intersecting two $\langle \bar{1}\bar{1}2\rangle$ sides of nanosheets, it is possible to achieve nanosheets with 1.5 times height of nonintersecting nanosheets.

Discussion. In this work, we have altered the shape of the opening in nanoscale SAG to be nanometer wide stripes aligned along the equivalent $\langle 11\bar{2}\rangle$ directions that promote the formation of {110} sidewall facets. Early stage nucleation in these stripes are tetrahedra with their axis pointing along the $\langle 11\bar{2}\rangle$ or $\langle \bar{1}\bar{1}2\rangle$ directions. These structures merge to form the final structures. However, twins are quickly formed at the initial stage of nanowire growth, and thus three inclined $(\bar{1}\bar{1}0)$ planes disappear while nanosheets maintain these inclined $(\bar{1}\bar{1}0)$ planes. Under growth conditions with higher AsH_3 partial pressures, mixed nucleation of $\langle 11\bar{2}\rangle$ or $\langle \bar{1}\bar{1}2\rangle$ oriented nuclei form, and the bounding planes are all inclined $(\bar{1}\bar{1}0)$ planes. There is a greater tendency for part of the structure to exhibit an apparent twinned region along the stripe that results from

dx.doi.org/10.1021/nl400561j | Nano Lett. 2013, 13, 2506−2515

the merger of $\langle \bar{1}\bar{1}2\rangle$ and $\langle 11\bar{2}\rangle$ oriented tetrahedron, as shown in the circled region of Figure 3a. However, if growth is carried out under nanosheet growth conditions at low AsH_3 partial pressures, nucleation of $\langle \bar{1}\bar{1}2\rangle$ oriented tetrahedra are not favored, and uniform nanosheets enclosed by three inclined $(\bar{1}\bar{1}0)$ planes and two vertical $(1\bar{1}0)$ planes are formed as shown in Figure 1b. Under such circumstances, the nanosheet is composed of only $\langle 11\bar{2}\rangle$ oriented tetrahedra, and no 180° rotation twins will be formed. Nearly twin-free nanostructures can thus be fabricated.

Growth behavior of GaAs nanosheets under different growth conditions was further studied; twinning in nanosheets was found significantly suppressed unlike nanowire structures which usually exhibit high twin density. The inherent property of frequent twin defects within nanowire structures made it difficult to investigate and analyze the cause of twinning. The morphology transition and facet formation of twinned nanosheets, by contrast, show the slow-down twinning process and thus made nanosheet the best platform for studying twinning. From our nanosheet study, twinning depends on both the thermodynamics and kinetics of the selective area growth.

In Figure 3, twinned or twin-free nanosheets can be formed under certain range of AsH_3 and TMGa partial pressures. Low AsH_3 and high TMGa partial pressures are required for twin-free nanosheets; however such growth condition corresponds to quite low V/III ratio (less than 6) which does not fall in the range of nanowire growth conditions. Considering thermodynamics,[24] the driving force for twin formation is increased under low AsH_3 and high TMGa partial pressures. This observation confirms that twinning is driven by the high chemical energy of MOCVD precursors and is allowed thermodynamically.

The same growth condition for twin-free nanosheets was applied to round opening holes, and the yield of nanowire growth was found to be greatly reduced, where most of depositions were tetrahedron growth (shown in Supporting Information). In a pair of papers[20,21] from Hokkaido University, a model for formation of nanowires by selective area growth has been proposed; it is hypothesized that, under the conditions of growth (low temperature and high AsH_3 partial pressure) used for the formation of nanowires, tetrahedral nuclei bounded by {110} planes were aligned with the dominant axis of the tetrahedra pointing to the $\langle 11\bar{2}\rangle$ direction. Repetitive twinning results in the formation of the hexagonal structure which is characteristic of nanowires. In this scenario, if growth condition for twin-free nanosheets is applied to round opening nanopatterns, the nanowire structure is less likely to form (see Supporting Information). Such a phenomenon well supports Ikejiri's[20] model and may explain the difficulties of forming twin-free "hexagonal" nanowires by selective area growth.

Since round and stripe patterns result in different shapes of nanostructure growth, the twin formation in the nanostructures may be explained by their surface energy. The analysis of surface energy for nanowire vs nanosheet structures along with the change of surface energy due to twin formation may provide a clue for reducing twinning. Observing the morphology change of nanosheets during twin formation, three inclined $(\bar{1}\bar{1}0)$ planes are replaced by three (111)A planes which have a lower density of dangling bonds. Since surface energy is related to the density of dangling bonds, the enclosed surface of the nucleation tetrahedra changes from three inclined $(\bar{1}\bar{1}0)$ planes to (111)A planes resulting in a decrease of surface energy. Thus, twinning can provide a way to reduce surface energy. Due to the high surface/volume ratio of nanostructures, the influence of surface energy is more important than its bulk energy; thus twinning would be preferred if they can dramatically decrease surface energy of nanostructure by paying a small penalty—the formation energy of twins.

The effect of surface energy reduction from twinning for different patterns can thus be analyzed. In the following, total surface energy change is calculated before and after twin formation with the assumption that the GaAs nucleation is first defined by three inclined $\{\bar{1}\bar{1}0\}$ planes and then by three {111}A planes after the twin is formed: experimentally, the GaAs nanosheets without twins were observed to be bounded by $\{\bar{1}\bar{1}0\}$ planes, whereas the nanosheets with twins were found to be bounded by {111}A planes after regrowth on inclined planes. We begin by calculating the total surface energy of a nanowire; because a round pattern is used for nanowire, the surface energy of a tetrahedron is considered. Figure 6a shows the schematics of nanowire structure for twin-free and twinned cases. In the calculation, only a single twin is considered. The surface energy of semitetrahedron with height h is calculated for both twin-free and twinned cases; however in the twinned case, a single twin occurs just at the top surface of semitetrahedron: when the height of semitetrahedron equals to h, a single twin is formed, and after that the enclosed surfaces of semitetrahedron are changed. So total surface energy including the twin energy per unit volume (in the following, Avg_E will be used as an abbreviation) can be derived for both cases from following equations:

Twin-free:

$$[(① + ② + ③) \times E(-1 - 10) + ④ \times E(111)\mathrm{B}]/V_{\text{twin-free}}$$

Twinned:

$$[(①' + ②' + ③') \times E(111)\mathrm{A} + ④' \times E(111)\mathrm{B} + \mathrm{Twin_E}] / V_{\text{twin}}$$

Within above equations, ①, ②, and ③ denote the surface area of three inclined $(\bar{1}\bar{1}0)$ planes, and ④ denotes the surface area of top (111)B planes for the twin-free case; and ①′ to ③′ denote the surface area of three inclined (111)A planes, and ④′ denotes the surface area of top (111)B planes for the twinned case. $E(\bar{1}\bar{1}0)$, $E(111)$A, and $E(111)$B denote surface energies of $(\bar{1}\bar{1}0)$, (111)A, and (111)B surfaces of GaAs. Figure 7a shows the calculated Avg_E for both cases with surface energy of different facets from Sibirev's[25] study; the radius of the round pattern is set to 150 nm. In the figure, the Avg_E of semitetrahedron with and without a single twin at different h is plotted. As can be seen, the Avg_E of the twinned case is always lower than that of twin-free case, and the difference increases dramatically when h approaches 50 nm which is the height of the apex of {110} bounded tetrahedron. Thus, surface energy considerations always favor twin formation during nanowire growth because it reduces surface energy of tetrahedral nuclei. From Figure 6a, surface energy difference increases dramatically when it reaches the apex of the tetrahedron which means that twin is more favored at the apex; thus larger opening holes would help to decrease twin density because it can postpone a dramatic increase in the energy differences. This trend is essentially what Ikejiri[20] found. Similar calculations are also performed for the nanosheet

dx.doi.org/10.1021/nl400561j | Nano Lett. 2013, 13, 2506−2515

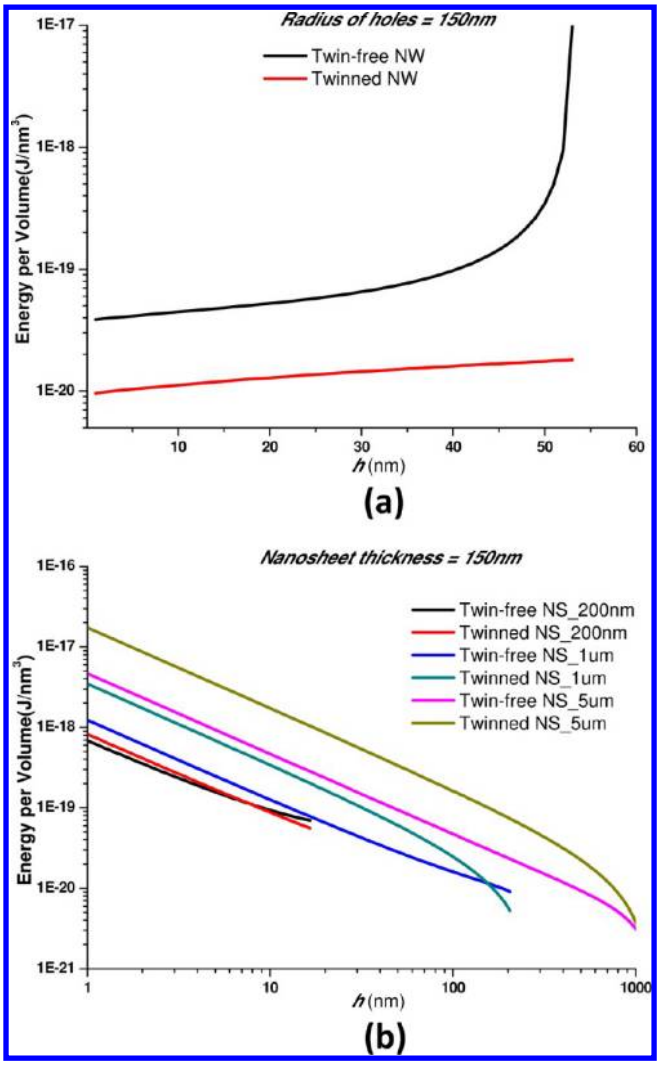

Figure 7. (a) Total surface energy plus twin energy per unit volume for twin-free and twinned nanowire structures. (b) Total surface energy plus twin energy per unit volume for twin-free and twinned nanosheet structures with different lengths.

structure: schematic diagrams of twin-free and twinned nanosheets are shown in Figure 6b, and Avg_E for both cases are calculated from the following equations:

Twin-free:

$$[(① + ② + ③ + ⑤ + ⑥) \times E(-1 - 10) + ④ \times E(111)\mathrm{B}]/V_{\text{twin-free}}$$

Twinned:

$$[(①' + ②' + ③') \times E(111)A + ④' \times E(111)B + (⑤' + ⑥') \times E(-1 - 10) + \mathrm{Twin_E}]/V_{\text{twin}}$$

Figure 7b shows the Avg_E of nanosheets with different lengths. The thickness of nanosheet is set to 150 nm in the calculation. The trend of Avg_E is different in nanosheets structures: Avg_E of the twin-free case is lower than that of twinned case for a range of h values for the nanosheet structure of different lengths as shown in Figure 7b. Therefore, compared to nanowire structure, twin formation is not energetically favored in the nanosheet structure. Thus, twin-free nanosheets can be formed. When the length of the nanosheet increases, the Avg_E difference between twin-free and twinned cases increases which means that the height of twin-free portion of nanosheet can be increased with longer nanostripe patterns. As shown in Figure 7b, the Avg_E of twin-free and twinned case intersects at specific height h and after that the Avg_E of twinned case becomes lower. That specific height h is very close to the height of nanosheet's tip. This helps to illustrate why twinning is likely to occur near the tip of nanosheets similar to what is observed in Figure 4a. From above, a model based on minimization of the surface energy seems to explain the tendency for nanowires to form twins and for nanosheets to form without them. Since the influence of surface energy is more significant in nanostructures, twin defects become favored if the structure formed reduces the surface energy more than the penalty energy it incurs in forming the twin. In a nanowire structure, three {110} planes of a tetrahedron turn into three {111} planes after twin formation; thus surface energy is greatly lowered with twin defects. However, due to the confinement of the nanostripe, a nanosheet has two stable vertical $(1\bar{1}0)$ planes that will not be transformed into {111} planes when a twin occurs. Since the area of these two vertical planes is the majority part of total surface area in the nanosheets structure, the surface energy reduction resulting from twinning is not as dramatic as that in the nanowire structure. From the point of view of kinetics, this appears to explain why the nanosheet structure has a lower twin probability than nanowire structure.

Similar nanostructures: InAs nanomembranes[26] which also have two vertical {110} planes have been grown on (100) Si using SAG. Unlike the GaAs nanosheet structure, the InAs nanomembrane is not a twin-free structure even though the surface area of two vertical {110} planes is also the majority of nanomembrane structure. It seems that large surface of {110} planes do not help to suppress twinning effect in the InAs nanomembrane structure. However, aside from influence of the {110} planes, other conditions could also influence the formation of twins, such as V/III and growth temperature. Another possible reason that differentiates InAs nanomembrane and GaAs nanosheet is the nucleation mechanism: nanomembranes first initialize from a rectangular pyramidal island nucleus and then two arms which show high twin density extend along two opposite ⟨111⟩B directions; these two arms were nucleated from tiny (111)B surfaces of a rectangular pyramidal island which is similar to nanowire growth. Therefore, just as the calculation shown above, two arms of nanomembranes could have higher twin density compared to nanosheet structure which nucleates from elongated nanostripe pattern.

Surface energy reduction is the likely cause of high density of twins observed within Sag grown GaAs nanostructures. If there is a way to avoid or eliminate the surface energy reduction caused by twinning, there may be ways to form other twin-free nanostructures like the nanosheet. It is still unknown why the starting form of tetrahedron is bounded by {110} planes rather than {111} planes even though {111} surfaces have lower energy. From the observed morphology transition that occurs in nanosheets upon twin formation as shown in Figure 4f, surface energy reduction actually comes after formation of a kink at the boundary of the twin. The formation of {111} planes seems require the formation of kinks. If there is a way to form a kink without twins, or if it is possible to grow {111} bounded nuclei directly, surface energy reduction would be achieved without the occurrence of twinning; therefore it may be possible to form SAG grown twin-free nanowires.

dx.doi.org/10.1021/nl400561j | Nano Lett. 2013, 13, 2506−2515

Conclusions. Several reports have revealed twin-free GaAs nanostructures by vapor−solid−liquid growth techniques; however twin-free nanostructures have not previously been observed when formed by selective area growth techniques. GaAs nanosheets grown on (111)B GaAs substrates are the first twin-free GaAs nanostructures grown by SAG technique. From the study of nanosheets, two ways to reduce twinning are suggested: first is using thermodynamic method by operating under growth conditions which result in a low driving force for twinning effect. The second method is using specifically designed patterns like the nanostripe within which the contribution to the surface energy of the two vertical planes increases that mitigates the surface energy benefit brought by twin formation and thus makes twinning less favored from the kinetics point of view. From the study of twinning effects in nanosheets, forming {111} bounded tetrahedron nuclei or growing kinks without twins could be the possible solution to SAG grown twin-free nanowires. Further studies of nanosheets will be focused on the optical and electrical properties.

■ ASSOCIATED CONTENT

Ⓢ Supporting Information

SEM images of SAG on round opening holes with twin-free nanosheet growth conditions. This material is available free of charge via the Internet at http://pubs.acs.org.

■ AUTHOR INFORMATION

Notes

The authors declare no competing financial interest.

■ ACKNOWLEDGMENTS

This work was supported by the Center for Energy Nanoscience (CEN), an Energy Frontier Research Center (EFRC) funded by the U.S. Department of Energy, Office of Science and Office of Basic Energy Sciences, under Award Number DE-SC0001013. S.H. would like to acknowledge the funding supported through the Office of Science of the U.S. Department of Energy under Award No. DE-SC0004993 to the Joint Center for Artificial Photosynthesis, a DOE Energy Innovation Hub.

■ REFERENCES

(1) Huang, Y.; Duan, X.; Cui, Y.; Lauhon, L. J.; Kim, K. H.; Lieber, C. M. *Science (New York, N.Y.)* **2001**, *294*, 1313−7.
(2) Bertness, K. A.; Kurtz, S. R.; Friedman, D. J.; Kibbler, A. E.; Kramer, C.; Olson, J. M. *Appl. Phys. Lett.* **1994**, *65*, 989.
(3) Takamoto, T.; Ikeda, E.; Kurita, H.; Ohmori, M. *Appl. Phys. Lett.* **1997**, *70*, 381.
(4) Wang, J.; Gudiksen, M. S.; Duan, X.; Cui, Y.; Lieber, C. M. *Science (New York, N.Y.)* **2001**, *293*, 1455−7.
(5) Tomioka, K.; Motohisa, J.; Hara, S.; Fukui, T. *Nano Lett.* **2008**, *8*, 3475−80.
(6) Tomioka, K.; Kobayashi, Y.; Motohisa, J.; Hara, S.; Fukui, T. *Nanotechnology* **2009**, *20*, 145302.
(7) Plissard, S.; Dick, K. A.; Larrieu, G.; Godey, S.; Addad, A.; Wallart, X.; Caroff, P. *Nanotechnology* **2010**, *21*, 385602.
(8) Heiss, M.; Conesa-Boj, S.; Ren, J.; Tseng, H.-H.; Gali, A.; Rudolph, A.; Uccelli, E.; Peiró, F.; Morante, J.; Schuh, D.; Reiger, E.; Kaxiras, E.; Arbiol, J.; Fontcuberta i Morral, A. *Phys. Rev. B* **2011**, *83*, 1−10.
(9) Perera, S.; Fickenscher, M. A.; Jackson, H. E.; Smith, L. M.; Yarrison-Rice, J. M.; Joyce, H. J.; Gao, Q.; Tan, H. H.; Jagadish, C.; Zhang, X.; Zou, J. *Appl. Phys. Lett.* **2008**, *93*, 053110.
(10) Kang, J.; Gao, Q.; Joyce, H. J.; Tan, H. H.; Jagadish, C.; Kim, Y.; Guo, Y.; Xu, H.; Zou, J.; Fickenscher, M. A.; Smith, L. M.; Jackson, H. E.; Yarrison-Rice, J. M. *Cryst. Growth Des.* **2011**, *11*, 3109−14.
(11) Thelander, C.; Caroff, P.; Plissard, S.; Dey, A. W.; Dick, K. A. *Nano Lett.* **2011**, *11*, 2424−9.
(12) Schroer, M. D.; Petta, J. R. *Nano Lett.* **2010**, *10*, 1618−22.
(13) Joyce, H. J.; Gao, Q.; Tan, H. H.; Jagadish, C.; Kim, Y.; Zhang, X.; Guo, Y.; Zou, J. *Nano Lett.* **2007**, *7*, 921−6.
(14) Joyce, H. J.; Wong-Leung, J.; Gao, Q.; Tan, H. H.; Jagadish, C. *Nano Lett.* **2010**, *10*, 908−15.
(15) Joyce, H. J.; Gao, Q.; Tan, H. H.; Jagadish, C.; Kim, Y.; Fickenscher, M. A.; Perera, S.; Hoang, T. B.; Smith, L. M.; Jackson, H. E.; Yarrison-Rice, J. M.; Zhang, X.; Zou, J. *Nano Lett.* **2009**, *9*, 695−701.
(16) Gorji Ghalamestani, S.; Ek, M.; Ganjipour, B.; Thelander, C.; Johansson, J.; Caroff, P.; Dick, K. A. *Nano Lett.* **2012**, *12*, 4914−9.
(17) Vu, T. T. T.; Zehender, T.; Verheijen, M. A.; Plissard, S. R.; Immink, G. W. G.; Haverkort, J. E. M.; Bakkers, E. P. A. M. *Nanotechnology* **2013**, *24*, 115705.
(18) Shtrikman, H.; Popovitz-Biro, R.; Kretinin, A.; Houben, L.; Heiblum, M.; Bukała, M.; Galicka, M.; Buczko, R.; Kacman, P. *Nano Lett.* **2009**, *9*, 1506−10.
(19) Shtrikman, H.; Popovitz-Biro, R.; Kretinin, A.; Heiblum, M. *Nano Lett.* **2009**, *9*, 215−9.
(20) Ikejiri, K.; Sato, T.; Yoshida, H.; Hiruma, K.; Motohisa, J.; Hara, S.; Fukui, T. *Nanotechnology* **2008**, *19*, 265604.
(21) Yoshida, H.; Ikejiri, K.; Sato, T.; Hara, S.; Hiruma, K.; Motohisa, J.; Fukui, T. *J. Cryst. Growth* **2009**, *312*, 52−7.
(22) Chu, H.-J.; Yeh, T.-W.; Stewart, L.; Dapkus, P. D. *Phys. Status Solidi C* **2010**, *7*, 2494−2497.
(23) Chang, C.-C.; Chi, C.-Y.; Yao, M.; Huang, N.; Chen, C.-C.; Theiss, J.; Bushmaker, A. W.; Lalumondiere, S.; Yeh, T.-W.; Povinelli, M. L.; Zhou, C.; Dapkus, P. D.; Cronin, S. B. *Nano Lett.* **2012**, *12*, 4484−9.
(24) Stringfellow, G. B. *Organometallic Vapor-Phase Epitaxy: Theory and Practice*, 2nd ed.; Elsevier: New York, 1999.
(25) Sibirev, N. V.; Timofeeva, M. A.; Bol'shakov, A. D.; Nazarenko, M. V.; Dubrovskiĭ, V. G. *Phys. Solid State* **2010**, *52*, 1531−8.
(26) Conesa-Boj, S.; Russo-Averchi, E.; Dalmau-Mallorqui, A.; Trevino, J.; Pecora, E. F.; Forestiere, C.; Handin, A.; Ek, M.; Zweifel, L.; Wallenberg, L. R.; Rüffer, D.; Heiss, M.; Troadec, D.; Dal Negro, L.; Caroff, P.; Fontcuberta i Morral, A. *ACS Nano* **2012**, *6*, 10982−91.